Excitation Dynamics in the LHCII Complex of Higher Plants: Modeling Based on the 2.72 Å Crystal Structure

Vladimir I. Novoderezhkin,[†] Miguel A. Palacios,[‡] Herbert van Amerongen,[§] and Rienk van Grondelle*[,‡]

A. N. Belozersky Institute of Physico-Chemical Biology, Moscow State University, Leninskie Gory, 119992 Moscow, Russia, Department of Biophysics, Faculty of Sciences, Vrije Universiteit, De Boelelaan 1081, 1081 HV Amsterdam, The Netherlands, and Laboratory of Biophysics, Department of Agrotechnology and Food Sciences, Wageningen University, Dreijenlaan 3, 6703 HA Wageningen, The Netherlands

Received: December 29, 2004; In Final Form: March 3, 2005

We have modeled steady-state spectra and energy-transfer dynamics in the peripheral plant light-harvesting complex LHCII using new structural data (Liu, Z.; Yan, H.; Wang, K.; Kuang, T.; Zhang, J.; Gui, L.; An, X.; Chang, W. *Nature.* **2004**, *428*, 287). The dynamics of the chlorophyll (Chl) *b*→Chl *a* transfer and decay of selectively excited "bottleneck" Chl *a* and *b* states have been studied by femtosecond pump−probe spectroscopy. We propose an exciton model of the LHCII trimer (with specific site energies) which allows a simultaneous quantitative fit of the absorption, linear-dichroism, steady-state fluorescence spectra, and transient absorption kinetics upon excitation at different wavelengths. In the modeling we use the experimental exciton−phonon spectral density and modified Redfield theory. We have found that fast *b*→*a* transfer is determined by a good connection of the Chls *b* to strongly coupled Chl *a* clusters, i.e., *a*610−*a*611−*a*612 trimer and *a*602−*a*603 and *a*613−*a*614 dimers. Long-lived components of the energy-transfer kinetics are determined by a quick population of red-shifted Chl *b*605 and blue-shifted Chl *a*604 followed by a very slow (3 ps for *b*605 and 12 ps for *a*604) flow of energy from these monomeric bottleneck sites to the Chl *a* clusters. The dynamics within the Chl *a* region is determined by fast (with time constants down to sub-100 fs) exciton relaxation within the *a*610−*a*611−*a*612 trimer, slower 200−300 fs relaxation within the *a*602−*a*603 and *a*613−*a*614 dimers, even slower 300−800 fs migration between these clusters, and very slow transfer from *a*604 to the quasi-equilibrated *a* sites. The final equilibrium is characterized by predominant population of the *a*610−*a*611−*a*612 cluster (mostly the *a*610 site). The location of this cluster on the outer side of the LHCII trimer probably provides a good connection with the other subunits of PSII.

Introduction

During the past decade, the study of the energy-transfer dynamics in the peripheral light-harvesting complexes from higher plants has attracted much effort[1] following the discovery in 1994 of the crystal structure of the major antenna complex LHCII.[2] The LHCII structure was modeled with 3.4 Å resolution, which did not allow for a distinction between chlorophyll (Chl) *a* and *b* or between the *X* and *Y* axes of the Chls. Thus, the identities of the Chls at the 12 discernible binding sites and the direction of their dipole moments could only be assigned in a hypothetical fashion.

Several site-directed mutagenesis studies of the chlorophyll binding residues have been carried out to determine the Chl identities in LHCII[3−6] and in the similar complex CP29.[7,8] It was concluded that five sites are occupied by Chls *a*, three sites by Chls *b*, and four sites are "mixed", i.e., can bind both Chls *a* and Chls *b*. Modeling of the steady-state spectra with exciton theory allowed several plausible configurations of the antenna to be found (including identities, site energies, and orientations of the 12 Chls).[9−12]

The dynamical behavior of LHCII, specifically the energy transfer between the chlorophylls, was studied with various time-resolved nonlinear spectroscopic methods. Transient absorption (TA) and time-resolved fluorescence studies revealed that Chl *b* to Chl *a* transfer takes place with two major time constants of ∼300 and ∼600 fs at 77 K [13−17] or ∼150 and ∼600 fs at room temperature[13,18−20] and a minor 4−9 ps component. Equilibration within the Chl *a* manifold occurs to a large extent within a few hundred femtoseconds, but upon blue-side excitation slow picosecond components are also observed.[14,16] Three-pulse photon echo peak shift (3PEPS) and transient grating (TG) measurements on LHCII at room temperature[21,22] gave the same time constants for the Chl *b*→Chl *a* transfer and Chl *a*−Chl *a* equilibration as the TA studies. Moreover, modeling of the data showed sub-picosecond Chl *b*→Chl *b* transfer.[21,22] A quantitative picture was further developed[11] using a simultaneous fit of the steady-state spectra, TA, TG, and 3PEPS kinetics with the Redfield relaxation theory.[23,24] It was shown that the intraband (Chl *b*→Chl *b* and Chl *a*→Chl *a*) energy-transfer dynamics includes sub-picosecond (250−600 fs) exciton relaxation within dimeric or, in the Chl *a* band, more complicated clusters, sub-picosecond (600−800 fs) hopping between spatially separated clusters (in the *a* band), and "slow" (picosecond) migration between localized states. The interband (Chl *b*→Chl *a*) transfer is characterized by the presence of very fast channels, the fastest

* To whom correspondence should be addressed. Fax: +31-20-4447899. E-mail: rienk@nat.vu.nl.
[†] Moscow State University.
[‡] Vrije Universiteit.
[§] Wageningen University.

10.1021/jp044082f CCC: $30.25
Published on Web 04/28/2005

taking only 120 fs, which connect both localized and dimeric *b* states with the *a* band.[11]

In our previous work[12] two-color TA kinetics were measured at probe wavelengths from 641 to 689 nm with a step of 3 nm upon 650 nm excitation, thus allowing visualization of the evolution of the whole spectrum reflecting an interplay of the intra- and interband transfer in LHCII. The experiments provided evidence for long-lived states in the spectral region near 665−670 nm (i.e., between the absorption peaks of Chl *b* and Chl *a* at 650 and 675 nm, respectively), in agreement with earlier observations.[14,16] Modeling with the standard[23,24] and modified Redfield theory[25] allowed us to assign these "bottleneck" states and to explore their participation in the overall energy-transfer dynamics.[12] In our modeling these states are determined by two or three (depending on the model) monomeric Chls *a* or *b* shifted to the spectral region of 655−670 nm.

Recently the structure of the LHCII complex has been obtained at 2.72 Å resolution.[26] The 14 chlorophylls (Chl) found in each monomeric subunit were unambiguously assigned as 8 Chls *a* and 6 Chls *b*, and no indication for mixed binding sites was found. Also the orientations of the Chl molecules were determined. In the current paper we model the linear steady-state spectra and TA kinetics upon different excitation wavelengths using this new structure. We propose an exciton model (with specific site energies of the 14 Chls) which allows a quantitative fit of the data with the same approach (modified Redfield with experimental spectral density) as that previously used.[12] This new model is compared with the configurations proposed earlier[11,12] on the basis of the old structure.[2]

The Model

We consider a trimeric LHCII complex with monomeric subunits consisting of 14 Chl molecules at sites *b*601, *a*602−*a*604, *b*605−*b*609, and *a*610−*a*614 (nomenclature from Liu et al.[26]). We suppose that the unperturbed site energies E_1-E_{14} of the 14 Chls within a monomeric subunit can be different, but the E_1-E_{14} set is the same for each of the three subunits within a trimer. The E_1-E_{14} values are free parameters for our modeling.

We use the same model as in our previous work.[12] The only differences appear due to the use of the new structure. Besides new pigment assignments, positions, and orientations, the new structure also suggests stronger coupling between pigment from different monomeric subunits. Thus, we use the full 42×42 one-exciton Hamiltonian for the trimeric complex with the site energies E_1-E_{14} as free parameters and the pigment−pitment interaction energies calculated in the dipole−dipole approximation. The static disorder (site inhomogeneity) is modeled by uncorrelated diagonal Gaussian disorder (full width at half-maximum (fwhm) of 80 cm^{-1} for Chls *a* and 95 cm^{-1} for Chls *b* as determined from the fit of the spectra). Although the unperturbed site energies E_1-E_{14} are the same for each of the three subunits, the random shifts of the site energies are different for all of the 42 Chls of the trimeric complex. This disorder produces a disorder of the pure exciton eigenvalues (which is less than in the site representation due to motional narrowing). In the presence of phonons these eigenstates will be further shifted due to phonon-induced reorganization effects.[12] The value of this shift is proportional to the participation ratio, thus depending on the specific realization of the disorder. As a result the "visible" inhomogeneity reflects the combined action of purely excitonic disorder and disorder due to reorganization shifts, a feature explicitly included into our model.[12] The strong exciton−phonon coupling is accounted for by using the spectral density modeled by a sum of overdamped Brownian oscillator (with coupling λ_0 and damping constant γ_0) and 48 high-frequency modes with frequencies ω_j, couplings $\lambda_j = S_j\omega_j$ (where S_j is the Huang−Rhys factor of the *j*th mode), and damping constants γ_j. The couplings λ_0 and λ_j are supposed to be site-independent but, for the Chls *b*, are taken to be 1.15−1.35 (depending on the model) times larger than for Chls *a* (within Chl *b* and *a* manifolds they are taken to be constant). In our previous study[12] these parameters were taken from experimental FLN data for LHCII[28] and further scaled and adjusted from the fit of the linear spectra. Here we use exactly the same spectral density.

The effective dipole strength of Chls is estimated as f^2d^2/ϵ (where *d* is the vacuum transition dipole, *f* is the local field correction factor, and ϵ is the relative dielectric constant). For the light-harvesting Chls we suppose $\epsilon = n^2$, where $n = 1.54$ is the refractive index of the protein. In a recent study by Knox and Spring,[27] it was shown that $f^2d^2 = 33.1$ and 24 D^2 for Chl *a* and Chl *b*, respectively (at $n = 1.54$). Then, the effective dipole strength for Chl *a* equals $f^2d^2/n^2 = 13.9$ D^2. This value corresponds to the Q_y "0−0" transition, so that the full strength of the Q_y transition is probably 20% larger (as pointed out in ref 27). In our study the effective dipole strength for Chl *a* is varied in the 14−18 D^2 range (with the corresponding scaling of the Chl *b* dipole strength). The best fit of the linear spectra and nonlinear kinetics was obtained for a value of 16 D^2.

The TA kinetics are calculated using the doorway-window representation and modified Redfield theory (as was described in detail in ref 12). As in previous papers[11,12] we calculate the two-exciton states taking into account the contribution from the double-excited monomeric states. The energy of the S_1-S_2 transition was supposed to be 100 cm^{-1} blue-shifted with respect to that of the S_0-S_1 transition. The ratio between the dipole moments of the S_1-S_2 and S_0-S_1 transitions was varied from 0.4 to 1.2, giving the best fit of the TA spectral shapes for a ratio of 0.65.

To obtain the site energies (and adjust other parameters of the model), we use a simultaneous fit of the absorption (OD), linear dichroism (LD), steady-state fluorescence (FL) spectra, and transient absorption (TA) kinetics upon excitation at different wavelengths. Experimental OD and LD spectra were taken from ref 29, the FL spectra were taken from ref 30, and the TA measurements will be described elsewhere (Palacios et al., manuscript in preparation).

Results

Excitonic Interactions. The arrangement of the chlorophylls within the LHCII trimer according to the new crystal structure[26] is shown in Figure 1. The chlorophylls are arranged in two parallel layers lying close to the stromal or lumenal surface of the membrane. The layers are well-separated with an averaged distance between the chlorophylls of 17−18 Å. The shortest distance between two chlorophylls in the two layers is about 13.9 Å (between *b*609 and *b*606). There are strong exciton interactions between pigments within each layer, but there is no appreciable coupling between pigments belonging to different layers (as can be seen in Figure 2).

On the stromal side there are two tightly packed clusters of Chls *a* (encircled by red for one monomeric subunit), i.e., the trimer *a*610−*a*611−*a*612 and the dimer *a*602−*a*603. They are closely connected with three Chls *b* on the stromal side, Chls *b*601, *b*608, and *b*609. The structure suggests significant coupling between *b*601 and *b*609 from adjacent monomeric subunits. So, one can consider the *b*601−*b*608−*b*609 group

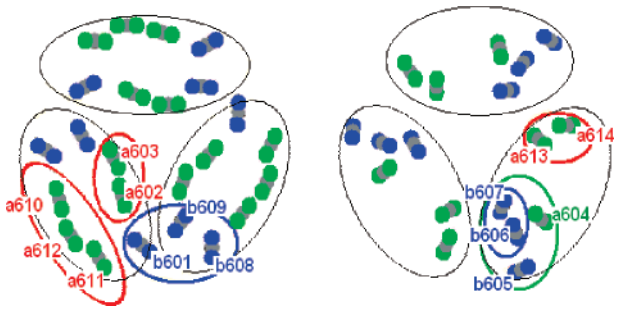

Figure 1. Arrangement of chlorophylls within an LHCII trimer at the stromal (left) and lumenal (right) sides. Chlorophylls are represented by three atoms: the central magnesium atom and two nitrogen atoms. The connecting line between the two nitrogens defines the directions of the Q_y transition dipole. Green, Chl *a* nitrogen; blue, Chl *b* nitrogen; gray, magnesium (according to the new structure reported by Liu et al.[26]). Clusters of Chl's *a*, Chl's *b*, and mixed groups containing long-lived intermediate sites are encircled by red, blue, and green, respectively.

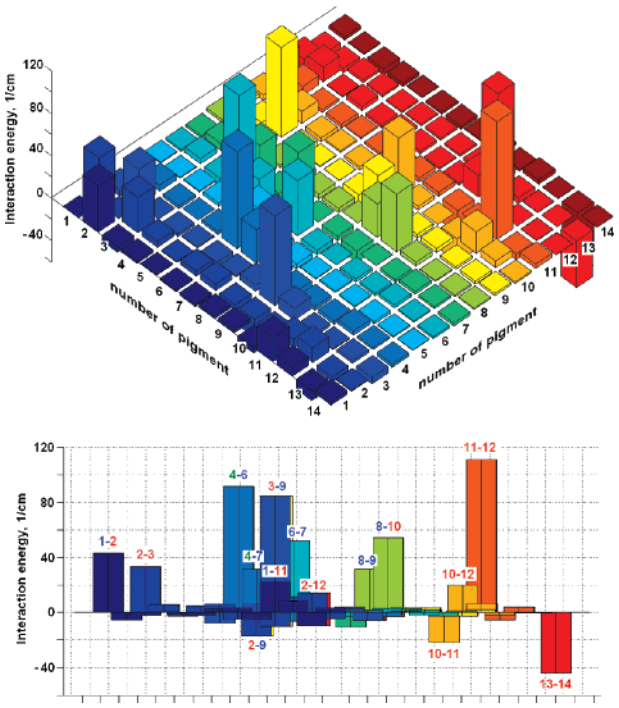

Figure 2. Off-diagonal part of the one-exciton Hamiltonian containing interaction energies M_{nm} for the pigments n and m ($n \neq m$) from one monomeric subunit. Pigments *b*601, *a*602, *a*603, ..., *a*614 are numbered as 1, 2, 3, ..., 14. In the bottom frame the strongest couplings ($|M_{nm}| >$ 14 cm^{-1}) are indicated. To distinguish between inter- and intraband interactions, the numbers are blue for *b* pigments and red for *a* pigments (or green for *a*604). Interaction energies correspond to the Chl *a* effective dipole strength of 14 D^2.

(encircled by blue in Figure 1) as a *b* cluster, which is expected to be short-lived due to transfer to the *a*610−*a*611−*a*612 and *a*602−*a*603 clusters of the two subunits. On the lumenal side there is a strongly coupled *a* cluster *a*613−*a*614 (encircled by red) and a mixed group of *a* and *b* sites (within the green circle). This mixed group (strongly coupled *b* cluster *b*606−*b*607, connected with the *b*605 and *a*604 pigments) is well-separated from the other pigments of the trimeric complex and also effectively decoupled from them due to fast energy transfer from the *b* sites to *a*604 (see below).

Interaction energies between pigments within one monomeric subunit are shown in Figure 2. In the bottom frame we indicate the strongest couplings (with absolute values larger than 14 cm^{-1}). Notice that Figure 2 does not contain interactions between pigments from adjacent monomeric subunits. The strongest of them, *b*601′−*b*609, equals 34 cm^{-1} (not to be confused with intramonomeric *b*601−*b*609 coupling, which is very weak as shown in Figure 2).

Within a monomeric subunit there are strong couplings within the Chl *a* clusters on the stromal side, i.e., within the *a*610−*a*611−*a*612 trimer (see interaction energies 11−12, 10−12, and 10−11 in the bottom frame of Figure 2) and the *a*602−*a*603 dimer (interaction 2−3). Pigments from the *b* cluster *b*601−*b*608−*b*609 are strongly coupled to the neighboring pigments from these two *a* clusters. The corresponding interband *a*−*b* interactions (3−9 plus 2−9 couplings for *b*609, 8−10 plus 8−3 for *b*608, and 1−2 plus 1−11 for *b*601) are stronger than the intraband *b*−*b* ones (8−9 and intermonomeric 1′−9 and 1′−8). Thus, the dynamics of interband *b*→*a* transfer in the LHCII trimer is not significantly influenced by interactions between monomeric subunits. This is in agreement with the conclusions drawn from the transient absorption measurements on monomeric and trimeric LHCII.[15] But, intermonomeric interactions may shift the exciton levels in the *b* region (as we will see in the next section). In the *a* region we expect fast exciton relaxation within the *a*610−*a*611−*a*612 and *a*602−*a*603 clusters as well as slower hopping between these clusters determined by 3−10, 2−11, and 2−12 interactions.

On the lumenal side there are two groups of pigments weakly coupled to each other and to pigments on the stromal side. First, the *a*613−*a*614 dimer is characterized by strong 13−14 coupling and by the absence of strong interactions with other pigments of the complex. Thus, there is only weak 1−13 connection within the *b* band and weak coupling (2−13, 10−13, and 3−14) with the *a* pigments on the stromal side. The second group contains strongly coupled *b*606 and *b*607 pigments with even stronger coupling to *a*604 (due to 4−6 interaction and a weaker 4−7 one) and with strong coupling to *b*605 (via 5−6 interaction which is as strong as the 4−7 one, but hidden under the 4−7 bar in the bottom frame of Figure 2). This group is a heterotetramer with strong interactions between three Chls *b* and one Chl *a* (but interaction between the *a*604 and *b*605 pigments is rather weak). All four pigments are weakly connected to the remaining part of the complex. Moreover due to very strong 4−6 coupling, the dynamics must be dominated by very fast downhill transfer of excitations from the *b* sites to the *a*604 pigment. The latter has only a very weak coupling with *a* pigments 2 and 10−12. Thus the *a*604 pigment is the best candidate for a long-lived bottleneck state, the presence of which was suggested in previous experimental[14−16] and theoretical[11,12] studies. Other pigments that can in principle contribute to a slow picosecond component of the kinetics[14−16,12] are *a*613, *a*614, and *b*605. In the model discussed below the *b*605 pigment gives the 3 ps component. The latter is different from the 12 ps decay component of *a*604, thus reflecting the fact that these two pigments are not in equilibrium even in the picosecond time scale (due to weak coupling between them).

The preliminary conclusions drawn here are based on an analysis of the structure and interaction energy values. Below we will revisit these points after a quantitative fit of the spectra and nonlinear kinetics of the complex.

Steady-State Spectra. A simultaneous fit of the linear spectra, i.e., OD, LD, and FL, can be obtained in many different ways using different sets for the site energies within a monomeric subunit (E_1−E_{14}). To explain the shoulder of the absorption spectrum near 660 nm, some of the *a* pigments should be blue-shifted. It is important that one or more of these blue states must be long-lived as evidenced by experiments with

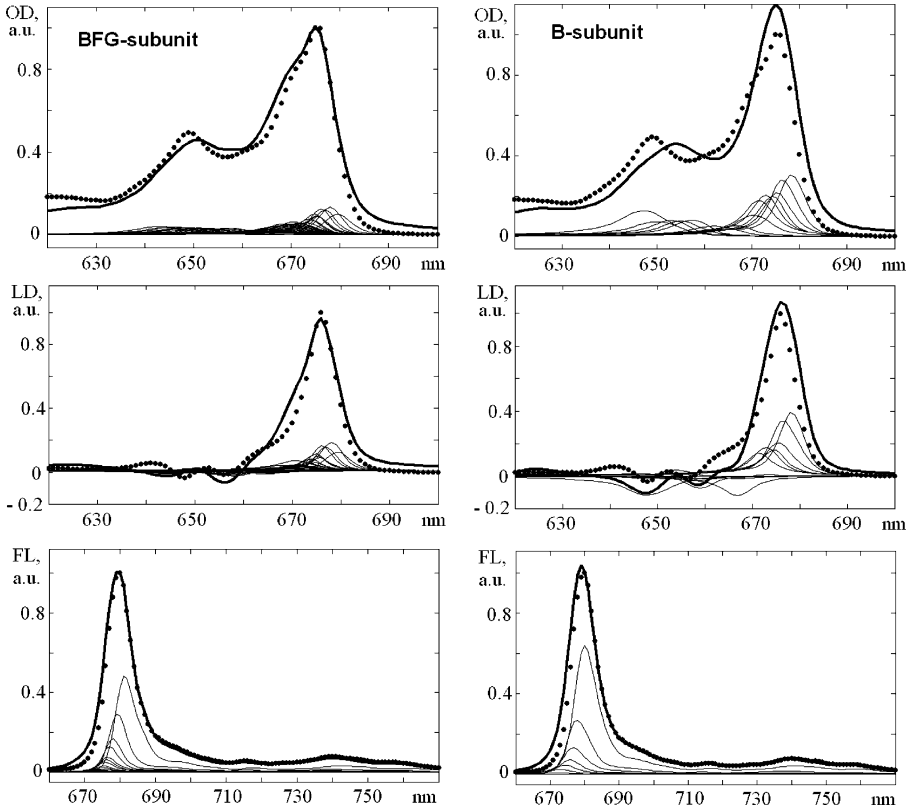

Figure 3. Experimental OD, LD, and FL spectra measured for LHCII trimer at 77 K (points) and the calculated ones (solid lines). Calculated spectra are shown together with individual exciton components (thin lines). Left frames: calculation for the trimer using assignments and orientations of the 42 Chl's of subunits B, F, and G (in notations of Liu et al.[26]). Site energies within monomeric subunit (E_1-E_{14}) have been adjusted in order to obtain the best fit (supposing the same distribution of the site energies for all three subunits). Right frames: the same as on the left, but the calculation was done without taking into account the interactions between pigments from different monomeric subunits.

selective excitation of the 660 nm region[14−16,12] This implies that they are spatially separated from other *a* pigments and are monomeric in nature. In principle, the shape of the OD, LD, and FL spectra can be explained if we shift some of the pigments from the strongly coupled *a* clusters. In this case the upper exciton level of the cluster can provide a component near 660 nm, but such a component cannot be long-lived due to fast exciton relaxation to a lower level within the same cluster. It seems that the new structure allows a unique solution to the problem, because there is only one monomeric *a* site, i.e., *a*604. Even if we fix the energy of *a*604 on the blue side of the *a* band, there are still a lot of possibilities to explain the shape of the linear spectra using different spectral positions of other *a* pigments.

Determination of the site energies from the OD/LD/FL fit has been performed using a simple evolutionary algorithm. We tried different initial sets of the site energies, i.e., equal energies for all pigments, random distribution of the site energies, and distributions with *a*604 blue-shifted. An evolutionary-strategy-based search for the best fit (minimizing the mean-square deviation) allows one to find two to three dozen models with different site energies. Further search gave configurations with approximately the same energies. These sets of site energies should be further checked by using them to fit the TA kinetics (see below).

An example of the OD, LD, and FL fit is shown in Figure 3. If we switch off the interactions between monomeric subunits, then the *b* band becomes red-shifted. The absence of the intermonomer excitonic interactions produces more localized *b* states with a larger reorganization energy shift. In addition, there are some changes in the excitonic structure of the *b* band producing changes in the *b* region of LD spectrum. In the *a* band the excitonic interactions between subunits do not change the delocalization within strongly coupled *a* clusters to an appreciable extent, but they lift the 3-fold degeneracy of these states, thus inducing some additional splitting. The spectrum of the monomeric subunit without these interactions is narrower in the *a* region (Figure 3). The experimental steady-state spectra of monomers and trimers were compared in detail by Nussberger et al.[31] The modeled changes upon monomerization appear to be different for the experimental spectra. The Chl *a* band is for instance broader for monomers, whereas the 660 nm band is less intense. There is no experimental red shift for Chl *b* in the absorption spectrum, and there are also some differences in the LD in the Chl *b* region. However, it is likely that some structural changes occur upon monomerization, and it appears that at least one Chl *a* is lost.[32]

It should also be remarked that although the shape of the simulated LD spectrum is very similar to that of the experimental one, the size is different. The absolute LD (difference in absorption for light polarized parallel and perpendicular to the plane of the trimer) was determined by analyzing the polarized absorption and fluorescence on partly oriented LHCII complexes.[29] The $LD_{max}/3OD_{max}$ ratio (where LD_{max} and OD_{max} correspond to the LD and OD maximums near 675 nm) is 0.47 in experiment[29] and 0.35 in the simulation. Note that the average LD in the Chl *a* region is not strongly dependent on the exciton model. It depends mostly on the orientation of the Q_y transition dipole moment within the plane of Chl *a*. The excitonic interactions within the *a* band only lead to a redistribution of the LD intensities over the spectrum. We have found that the $LD_{max}/3OD_{max}$ ratio for different models (which allow a good fit of the shape of linear spectra) is typically in the range of 0.31−0.37, i.e., lower than the experimental value. The origin

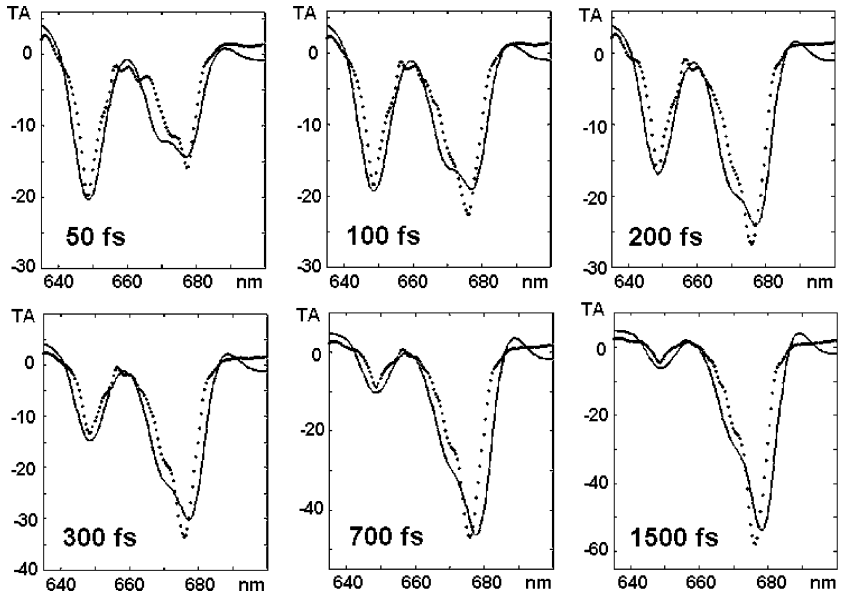

Figure 4. Two-color TA kinetics measured for LHCII at 77 K (points) and calculated with the modified Redfield theory (solid lines). Excitation wavelength, 650 nm; pulse duration, 90 fs; pump−probe delays, 50, 100, 200, 300, 700, and 1500 fs. Parameters of the model are the same as in the fit of linear spectra.

of this discrepancy is not clear at the moment. Assuming that the Chl orientations are correctly described by the crystal structure, one could suppose that the orientation of the Q_y transition dipoles may deviate from the *Y* axis of the Chl.

Notice that at this moment there is no good quantitative explanation for the circular dichroism (CD) spectrum of LHCII. The 77 K CD displays negative peaks at 648 and 677 nm and a broad structureless positive feature between 655 and 670 nm.[31] The modeling of Renger and May[9] based on the 1994 structure gave negative peaks at 644 and 680 nm and a positive band with three maxima at 655, 665, and 676 nm, in qualitative agreement with the experiment (but no quantitative fit was obtained). Our model (i.e., based on a new structure) predicts a very similar CD shape with negative peaks at 643 and 680 nm and a positive broad band with three peaks at 651, 665, and 675 nm (data not shown). We remark that the measured CD is strongly nonconservative, with a significant negative contribution, which seems to be proportional to the OD profile (probably due to a contribution from the monomeric CD). Also one could expect a mixing of the Q_y transitions with other electronic transitions of Chls and carotenoids. As a result, it is difficult to explain the data at a quantitative level. Thus, we did not include CD into our simultaneous fit of linear spectra.

Transient Absorption. The exciton models suggested by fitting of the linear spectra have been used for fitting of the TA spectra upon 650 and 662 nm excitation. Notice that calculation of the nonlinear response requires much more computing time (by 1−2 orders) as compared to the case of the linear spectra. That is why the evolutionary algorithm can be applied only for the OD/LD/FL fit. Calculation of the TA kinetics is used to accept or rule out models obtained from the linear spectra fit.

The 650 nm excitation creates population of the *b* band with subsequent energy transfer to the *a* region around 670−680 nm (an example of a fit is shown in Figure 4). Some of the models gave a wrong spectral shape of the TA (with significantly shifted peak positions or with nonrealistic widths of the bleaching peaks), and some models failed to reproduce the time scales of energy transfer (giving too fast or too slow $b \rightarrow a$ kinetics). Several models allowed a satisfactory fit. However, most of them have been ruled out after also considering the 662 nm kinetics. The 662 nm narrow-band excitation allows selective excitation of the intermediate blue-shifted *a* states. Thus the kinetics are much more sensitive to the fine structure of the blue wing of the *a* band. A simultaneous fit of the 650 and 662 nm TA is possible only with one model (this fit is shown in Figures 4 and 5). For this model we have performed a fine-tuning of the site energies. We have found that variation of the energies within ± 10 cm^{-1} is not critical with respect to the quality of the whole OD/LD/FL/TA fit. Of course, we cannot be absolutely sure that this final fit is the unique solution of the LHCII problem. One cannot exclude the existence of another good configuration with more or less the same site energies and a similar exciton structure. But (according to our experience), it seems highly unlikely that there exists an alternative model with significantly different site energies.

The site energies E_1-E_{14} for our best model are given in Table 1. The TA kinetics shown in Figures 4 and 5 are calculated using the trimeric model, i.e., taking into account all the interactions within the LHCII trimer. However, it is also possible to calculate the spectra and kinetics using a simplified monomeric model where the interactions between monomeric subunits are neglected. In this model the site energies should be adjusted (blue-shifted) in order to compensate for the larger reorganization red-shift. The intramonomeric exciton structure is given in Table 2. The site energies (given in Table 1) and the energies of the zero-phonon transitions of the exciton states (given in Table 2) have been determined from the fit with an accuracy of about 10 cm^{-1} as discussed above.

The lowest states $k = 1-2$ (see Table 2) are determined by the lowest exciton levels of the *a*610−*a*611−*a*612 cluster (680 nm) in our model. The noncoherent mixture of these levels with the lowest levels of the asymmetric dimers *a*602−*a*603 and *a*613−*a*614 (see levels $k = 2-4$) results in the main absorption peak near 675 nm. Higher levels of the *a*602−*a*603 and *a*613−*a*614 dimers together with the *a*604 monomer contribute to the shoulder at 670 nm both in the OD spectrum and in the TA bleaching (levels $k = 5-7$). The shoulder in the OD near 660−662 nm is determined by a combined contribution from the blue-shifted *a*604 and red-shifted *b*605 (levels $k = 8-9$). Notice that higher states of the *a* band also contain contributions from upper exciton levels of the *a*610−*a*611−*a*612 cluster (levels $k = 7-8$). Levels $k = 10-14$ correspond to the *b* band.

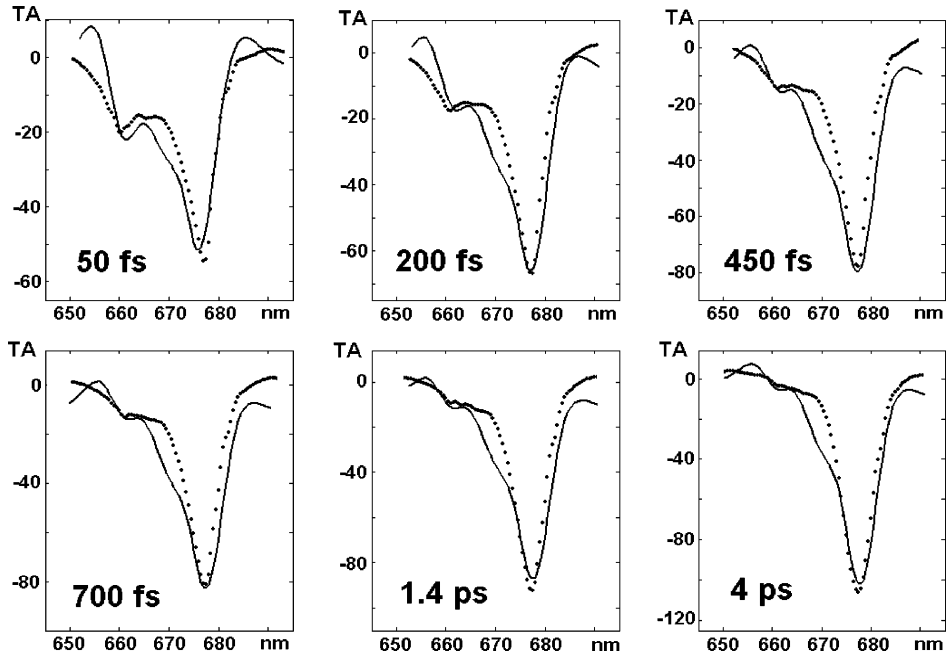

Figure 5. Same as in Figure 4 but for 662 nm excitation by 180 fs pulses. Pump−probe delays are 50, 200, 450, 700, 1400, and 4000 fs.

TABLE 1: Site Energies E_1-E_{14} for the LHCII Complex[a]

pigments	monomeric model			trimeric model		
*a*602−*a*603:	15 160	15 283		15 103	15 222	
*a*610−*a*611−*a*612:	15 073	15 115	15 097	15 038	15 100	15 082
*a*613−*a*614:	15 175	15 264		15 140	15 249	
*a*604:	15 460			15 410		
*b*601−*b*608−*b*609:	15 890	15 763	15 721	15 854	15 728	15 686
*b*605−*b*606−*b*607:	15 679	15 851	15 712	15 674	15 796	15 677

[a] The first set of energies corresponds to a simplified monomeric model where interactions between monomeric subunits are neglected. The second set was used to model the data with including all the interactions within LHCII trimer. The energies are given in cm^{-1} and do not include a reorganization energy shift.

Excitation of the *b* band at 650 nm is followed by fast sub-picosecond $b \rightarrow a$ transfer resulting in the formation of the bleaching band in the 670−680 nm region (Figure 4). Initially, the 670 nm shoulder is developing faster than the main 680 nm band due to effective population of the intermediate *a*604 site (which is most strongly coupled to the *b* pigments). After that, i.e., during formation of the 680 nm bleaching, the evolution of the 670 nm peak is slow due to weak coupling of *a*604 with other *a* pigments.

Notice that due to disorder the states $k = 5-7$ contain mixed *a*604, *a*603, and *a*614 contributions. This means that for different realizations of the disorder the eigenstate at any fixed wavelength within the 667−670 nm region can be the monomeric *a*604 state or the upper exciton level of the two asymmetric a dimers with predominant participation of *a*603 or *a*614. Thus, following 650 nm excitation the dynamics of the 670 nm bleaching band is determined by (i) fast population of *a*604, *a*603, and *a*614 from the *b* states (from 0 to about 1 ps delays), (ii) sub-picosecond exciton relaxation within the *a* dimers (with subsequent formation of the 680 nm bleaching band), and (iii) slow picosecond depopulation of *a*604.

A more direct visualization of the slow dynamics of intermediate states is possible upon selective narrow-band excitation of the 660−662 nm band. In our model the absorption at this wavelength is dominated by levels $k = 8-9$ with contributions from the blue-shifted *a*604, red-shifted *b*605, and higher exciton states of the *a*610−*a*611−*a*612 cluster. The corresponding TA dynamics is shown in Figure 5. Due to fast exciton relaxation within the *a*610−*a*611−*a*612 cluster one gets quick formation of the 680 nm bleaching already during the 180 fs pump pulse. Besides, selective excitation of the *b*605 and *a*604 sites leads to distinguishable bleaching features between 660 and 670 nm. The subsequent slow dynamics in the 660−670 nm region proves that the intermediate *a*604 and *b*605 are really long-lived bottleneck states.

Excitation Dynamics. We have seen that the time-dependent TA profiles can largely be explained in terms of the excited-state dynamics (including interband transfer, intraband exciton relaxation, and migration of localized excitations). Besides a fit of the TA, the model (specified in the previous section) also allows a direct visualization of the excitation dynamics in both the exciton (eigenstate) and site representation. The exciton picture provides the time-dependent population of one-exciton states of the complex. Figure 6 shows the one-exciton populations calculated with the monomeric model (Table 1). Excitation of the *b* band at 650 nm is followed by fast decay of the upper exciton states $k = 10-14$. Due to intraband equilibration (sub-picosecond exciton relaxation within *b* clusters) higher states exhibit faster decay. The next two states $k = 8-9$ are on the average long-lived due to the presence of intermediate sites *a*604 and *b*605. The next three states $k = 5-7$ are long-lived as well, again due to the contribution from *a*604 (see Table 2). The contribution of the upper exciton levels of the strongly coupled trimer *a*610−*a*611−*a*612 increases from the $k = 5$ to $k = 8$ state. Fast exciton relaxation reduces the population of the higher levels of this $k = 5-8$ group. Notice that the $k = 5-8$ states are also depopulated via exciton relaxation within the *a*602−*a*603 and *a*613−*a*614 dimers (higher states of these dimers

TABLE 2: Exciton Structure of LHCII Obtained with a Monomeric Model[a]

	$k=1$	$k=2$	$k=3$	$k=4$	$k=5$	$k=6$	$k=7$
E_{ZPL}	14 699	14 751	14 804	14 858	14 918	14 952	14 992
λ_{ZPL}	680	678	675	673	670	669	667
*b*601	0.04	0.05	0.06	0.06	0.03	0.06	0.07
*a*602	16.48	17.31	22.59	19.96	7.19	6.27	4.57
*a*603	1.14	2.51	5.92	11.09	33.65	17.41	13.94
*a*604	0.00	0.01	1.12	4.18	24.65	19.65	23.46
*b*605	0.00	0.00	0.00	0.00	0.00	0.00	2.24
*b*606	0.00	0.00	0.04	0.16	1.05	0.86	1.13
*b*607	0.00	0.00	0.01	0.02	0.14	0.12	0.17
*b*608	0.29	0.13	0.10	0.05	0.01	0.00	0.01
*b*609	0.06	0.12	0.25	0.42	1.21	0.61	0.50
*a*610	50.15	22.61	15.12	7.53	2.07	0.90	0.60
*a*611	10.31	20.15	12.01	6.19	4.21	10.74	16.27
*a*612	11.94	23.31	14.13	6.44	3.32	10.18	13.45
*a*613	8.82	12.08	23.99	28.04	7.02	7.13	5.86
*a*614	0.71	1.66	4.60	15.80	15.37	26.02	17.67
	$k=8$	$k=9$	$k=10$	$k=11$	$k=12$	$k=13$	$k=14$
E_{ZPL}	15 022	15 210	15 306	15 363	15 416	15 456	15 512
λ_{ZPL}	665	657	653	651	649	647	645
*b*601	0.10	19.13	32.09	27.12	8.27	9.32	3.54
*a*602	4.82	0.42	0.12	0.09	0.03	0.04	0.03
*a*603	9.69	1.29	0.39	0.57	1.04	0.78	0.48
*a*604	21.90	0.09	0.08	0.13	0.44	1.20	3.03
*b*605	1.68	52.80	17.42	10.33	7.34	5.31	2.84
*b*606	1.26	2.56	3.17	4.49	9.47	23.43	52.32
*b*607	0.42	12.96	24.42	22.03	15.63	13.49	10.52
*b*608	0.00	2.78	12.67	19.86	27.70	23.61	12.72
*b*609	0.34	4.97	9.47	15.16	29.83	22.62	14.38
*a*610	0.35	0.02	0.08	0.12	0.16	0.14	0.08
*a*611	19.44	0.55	0.03	0.02	0.00	0.01	0.00
*a*612	16.65	0.52	0.01	0.01	0.00	0.00	0.00
*a*613	6.47	0.53	0.01	0.01	0.00	0.00	0.00
*a*614	16.78	1.32	0.00	0.00	0.00	0.00	0.00

[a] For each of the 14 exciton levels ($k = 1-14$) the energies (cm^{-1}) and wavelengths (nm) of the zero-phonon transitions are given together with the participation of the pigments (%) averaged over realizations of the disorder.

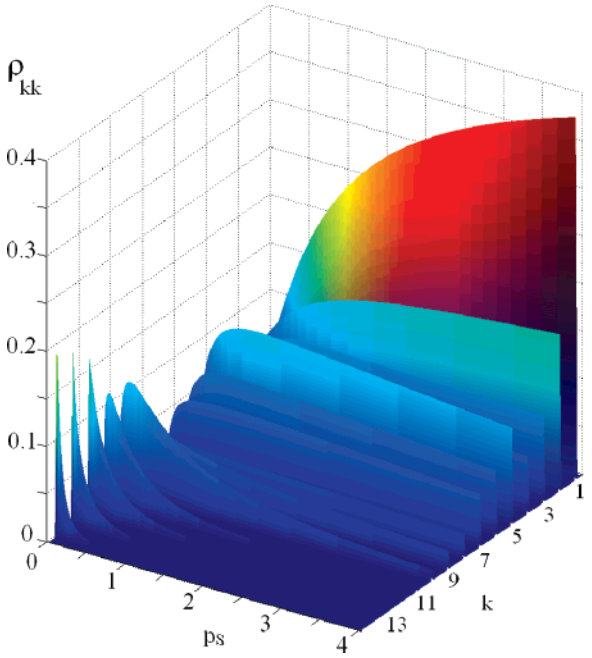

Figure 6. Dynamics of the one-exciton populations (averaged over disorder) at 77 K upon 650 nm excitation. The data were calculated with the monomeric model (see Table 1). Exciton states from $k = 1$ to 14 are arranged in increasing order of energy (with highest level in front of the figure).

contribute to the $k = 5-8$ states). But, the exciton relaxation within these dimers is not as fast as within the *a*610−*a*611−*a*612 cluster. The big difference in site energies (see Table 1) produces nonuniform delocalization (with localization at the *a*603 and *a*614 sites for the higher levels), thus reducing wave function overlap and intradimer relaxation rates. The states $k = 1-4$ are determined by the lowest exciton levels of the three *a* clusters. They exhibit fast population due to direct $b \rightarrow a$ transfer and exciton relaxation within the *a* band. The slow increase of their population is connected with slow transfer from the bottleneck sites *a*604 and *b*605.

Now we switch from the exciton to the site representation. Figure 7 shows the dynamics of the site populations calculated for the trimeric complex upon 650 nm excitation.

Three *b* sites on the stromal side (*b*601, *b*608, and *b*609) are characterized by fast sub-picosecond decay due to coupling to two *a* clusters (*a*610−*a*611−*a*612 and *a*602−*a*603). After 1 ps they are completely depopulated. Two *b* sites in the lumenal side (*b*606 and *b*607) show very fast (with components up to 100 fs) decay due to transfer to long-lived bottleneck sites (*b*605 and *a*604). After such sub-picosecond equilibration (within the *b*606−*b*607−*b*605−*a*604 group) the *b*605 and *a*604 pigments become highly populated (but nonuniformly due to the absence of strong coupling between them), whereas the *b*606 and *b*607 populations stay at some low, but nonzero, level. It is important that these quasi-equilibrated populations within this group of four pigments (encircled by green in Figure 1) show only very slow picosecond decay (in contrast to *b*601, *b*608, and *b*609) due to very weak coupling to the pigments outside the "green" area (Figures 1 and 2). Thus, a quick population of the bottleneck sites is followed by a very slow (3 ps for *b*605 and

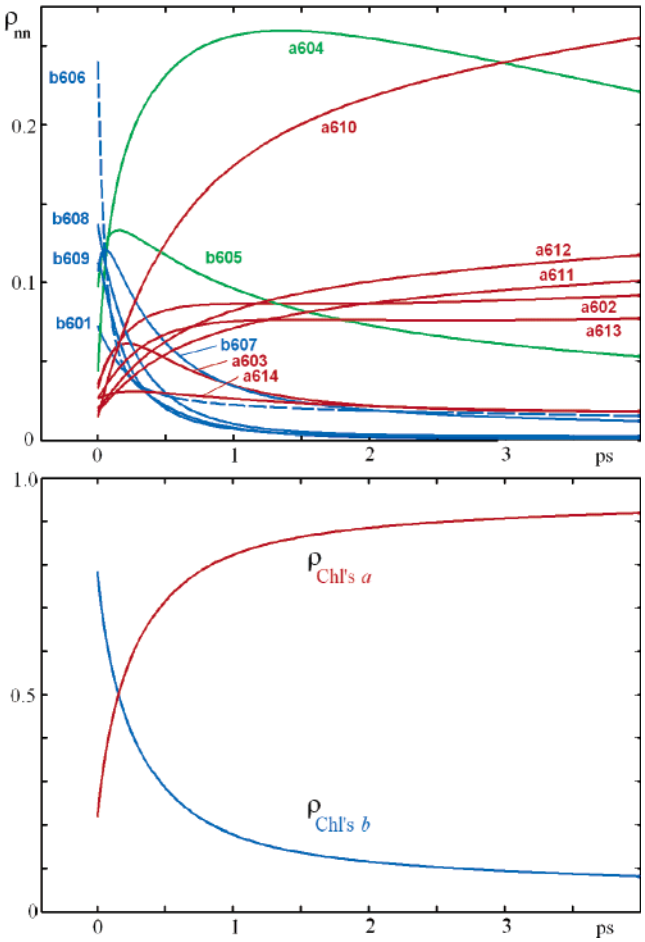

Figure 7. Dynamics of the site populations (averaged over disorder) at 77 K upon 650 nm excitation. Three groups of kinetics show populations of the *b* sites with fast decay (blue), *a* sites which contribute to the main absorption peak near 675 nm (red), and long-lived bottleneck sites (green), i.e., blue-shifted Chl *a* (*a*604) and red-shifted Chl *b* (*b*605). Bottom frame: Dynamics of populations of the whole *b* and *a* bands at 77 K upon 650 nm excitation (i.e. the sum of the corresponding curves shown in the top frame).

about 12 ps for *a*604) flow of energy to the remaining *a* sites. According to Table 2 the sites *b*605 and *a*604 contribute to the states with zero-phonon transitions at 657 and 665−670 nm, respectively. This determines the spectral distribution of the 3 and 12 ps components. This is in agreement with recent measurements giving components of a few picoseconds and 17 ps upon 660 and 670 nm excitation, respectively (Palacios et al., unpublished results).

The population of the main *a* pigments grows during the first picosecond due to transfer from Chl *b* sites. Slower components are dominated by equilibration within *a* clusters, hopping between clusters and very slow transfer from bottleneck states. As suggested above (in the analysis of the exciton representation dynamics) the equilibration within *a*602−*a*603 and *a*613−*a*614 dimers is slow (relative populations reach quasi-equilibrium only after 1.5−2 ps—see Figure 7). On the contrary, the relative populations of the *a*610−*a*611−*a*612 sites are almost constant after 100−200 fs (see also Figure 8), reflecting very fast exciton relaxation within this Chl trimer.

The dynamics of the population of the whole *b* and *a* bands upon 650 nm excitation is shown in Figure 7 (bottom frame). Time components are close to those known from the experiments at 77 K, i.e., 300 fs, 600 fs, and minor component of 4−9 ps.[13,18−20] Notice that 20% of the direct excitation of Chls *a* at $t = 0$ is caused by the overlap of the pump pulse with the vibronic wings of the *a* states.

In equilibrium a noncoherent mixing of the *a* clusters is obtained, i.e., depending on the realization of the disorder, one can find the excitation at the *a*610−*a*611−*a*612 (more often), the *a*602−*a*603, or the *a*613−*a*614 cluster. For our model (with the site energies obtained from a simultaneous fit of the steady-state and transient absorption spectra as shown in Figures 3 and 4) the averaging over disorder gives the predominant population of the *a*610−*a*611−*a*612 cluster (mostly *a*610). A location of this cluster on the outer side of the LHCII trimer is likely to provide a good connection with other subunits of PSII.

Figure 8 provides a visualization of the site population dynamics related to the positions within a monomeric subunit. The first three frames (0−700 fs) show the excitation-energy flow from the stromal-side Chls *b* (*b*601, *b*608, and *b*609) to the *a* sites and the redistribution of energy within the *a* clusters. Also redistribution within the lumenal-side *b*606−*b*607−*b*605−*a*604 group is clearly seen (with transfer from *b*606 to *b*607 and *b*605 and the predominant population of the intermediate *a*604 site). The next three frames (3−20 ps) show slow transfer from *a*604 (and from the *b*606−*b*607−*b*605 cluster) to the quasi-equilibrated *a* sites. Notice that *b*605 can be treated as a relatively long-lived bottleneck site together with *a*604 (in Figure 7 they are both marked in green). But, in Figure 8 it is more convenient to consider only *a*604 as a real bottleneck state.

Relaxation Rates. The excitation dynamics calculated above corresponds to the energy-transfer picture averaged over many realizations of the disorder. Calculation of the Redfield tensor shows that the relaxation rates are strongly dependent on the realization. In different realizations one can find not only different wave functions and energies, but also a different ordering of the exciton states. So, the transfer rate between any pair of states averaged over disorder will contain contributions with different time constants and also contributions from different relaxation pathways. Analysis of the Redfield tensor for particular realizations (with simultaneous assignment of the eigenstates) allows one to obtain the transfer rates for specific relaxation channels. In Table 3 we show the exciton structure and relaxation rates within the *a* region obtained for one realization of the disorder.

In Table 3 the $k = 1$, 5, and 8 states are exciton levels of the *a*610−*a*611−*a*612 cluster, $k = 2$ and 4 are exciton levels of the *a*602−*a*603 dimer, $k = 3$ and 7 are exciton levels of the *a*613−*a*614 dimer, and $k = 6$ is the monomeric *a*604 bottleneck state. There is some coherent superposition of the *a*613−*a*614 dimer and the *a*610−*a*611−*a*612 cluster in the $k = 7$ and 8 levels. There is also coherent admixture of the cluster *a*602−*a*603 to the $k = 3$ state (lowest state of the *a*613−*a*614 dimer) and to the $k = 5$ state (middle state of the *a*610−*a*611−*a*612 trimer).

Exciton couplings within and between clusters determine the rates of intracluster relaxation and intercluster migration. The fastest are relaxation channels within the *a*610−*a*611−*a*612 cluster, especially relaxation from the highest exciton level (which is typically the highest among all eight levels of the *a* region). In our example this is the case. As a result, the $k = 8$ level exhibits very fast decay. Thus, the rates of the $k = 8 \rightarrow 1$ and $8 \rightarrow 5$ relaxations are 11 and 4.5 ps^{-1}; i.e., time constants are 90 and 220 fs. Relaxation within the *a*613−*a*614 and *a*602−*a*603 dimers, i.e., $7 \rightarrow 3$ and $4 \rightarrow 2$ transfers, are not so fast. The corresponding time constants are 200 and 300 fs, respectively. The transfers between clusters are even slower, i.e., $8 \rightarrow 3$, $7 \rightarrow 1$,

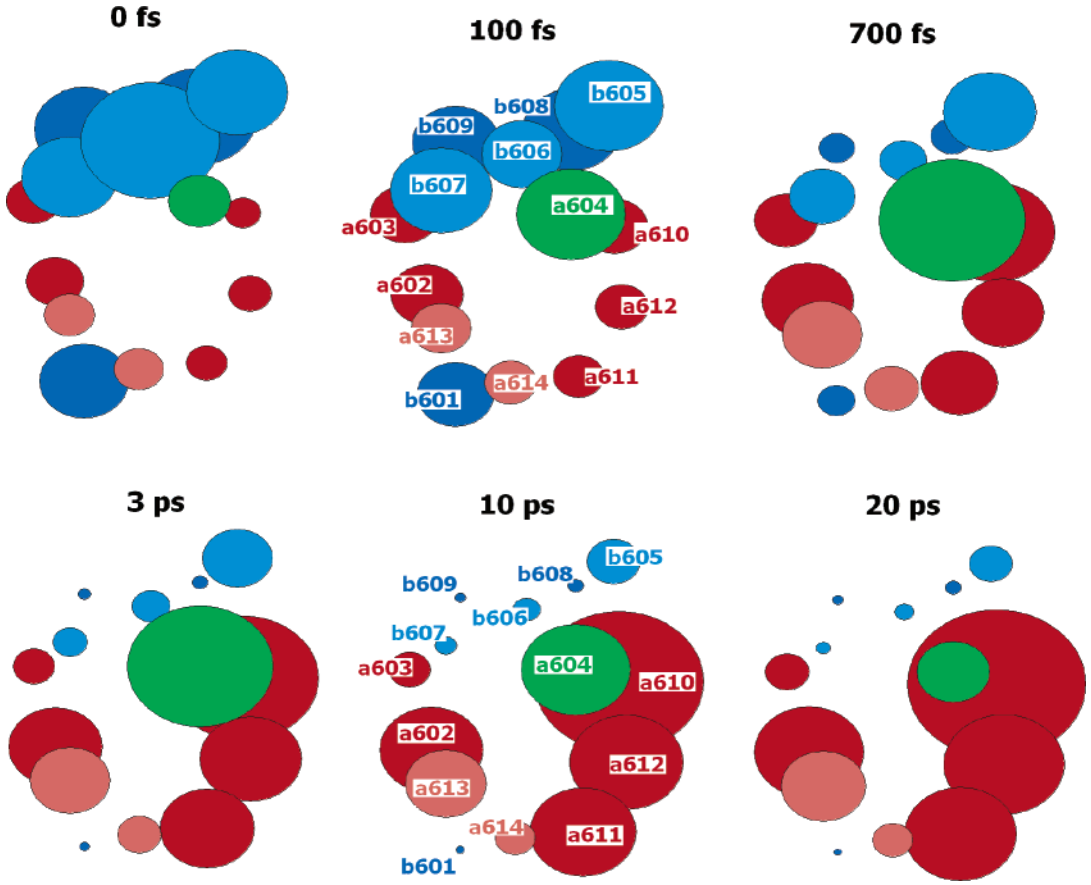

Figure 8. Dynamics of the site populations (averaged over disorder) during 0−20 ps upon 650 nm excitation at 77 K. The Chl sites within one monomeric subunit are shown by circles. The center of the circle corresponds to the position of the magnesium atom of the Chl molecule. The time-dependent area of the circle is proportional to a population of the corresponding site. Chls *a* in the stromal side (*a*602, *a*603, *a*610, *a*611, *a*612) are shown by red circles, Chls *a* in the lumenal side (*a*613, *a*614) are shown by light red, Chls *b* in the stromal side (*b*601, *b*608, *b*609) are blue, Chls *b* in the lumenal side (*b*605, *b*606, *b*607) are light blue, and the intermediate Chl *a* site in the lumenal side (*a*604) is shown by green.

TABLE 3: Exciton Structure and Relaxation Rates Obtained with a Monomeric Model of LHCII for One Particular Realization of the Disorder[a]

	$k=1$	$k=2$	$k=3$	$k=4$	$k=5$	$k=6$	$k=7$	$k=8$
*a*602	1.56	**68.56**	0.12	**26.49**	2.06	0.01	0.17	0.62
*a*603	0.70	**23.26**	1.75	**69.48**	2.29	0.00	0.31	0.03
*a*604	0.00	0.01	0.00	0.00	0.00	**94.48**	0.01	0.00
*a*610	**62.73**	5.53	0.29	0.10	**30.69**	0.00	0.01	**0.06**
*a*611	**14.99**	0.00	0.00	0.46	**28.03**	0.00	10.94	**45.41**
*a*612	**19.61**	1.11	0.13	0.01	**36.47**	0.01	9.70	**32.90**
*a*613	0.02	0.41	**76.50**	2.04	0.20	0.00	**15.67**	5.10
*a*614	0.00	0.00	**21.14**	0.02	0.00	0.01	**63.13**	15.66
$k'=1$	0.34	−0.33	−0.06	−0.41	**−1.86**	−0.01	***−1.36***	**−11.04**
$k'=2$	−0.13	2.92	***−1.97***	**−3.38**	−0.02	−0.02	−0.11	−0.14
$k'=3$	−0.02	−1.57	2.23	−0.12	−0.01	−0.00	**−5.17**	***−1.90***
$k'=4$	−0.05	−1.01	−0.04	6.14	***−2.90***	−0.00	−0.17	−0.26
$k'=5$	−0.10	−0.00	−0.00	−2.20	5.32	−0.01	−0.87	**−4.49**
$k'=6$	−0.00	−0.00	−0.00	−0.00	−0.00	0.08	−0.02	−0.00
$k'=7$	−0.01	−0.00	−0.13	−0.01	−0.08	−0.01	8.62	−0.69
$k'=8$	−0.02	−0.00	−0.01	−0.00	−0.13	−0.00	−0.20	18.56

[a] Participations of the *a* pigments (%) are shown for the lowest eight exciton states (upper part of the table). Bold font shows coherent superposition of pigments in the exciton states of the two dimers and one trimer in the *a* band. Underlined bold shows monomeric bottleneck state. The second part of the table shows the rates for the $k \rightarrow k'$ relaxation (ps^{-1}). Bold shows exciton relaxation rates within clusters, and italic bold shows intercluster transfer rates. Diagonal elements (underlined) correspond to the inverse lifetime of the *k*th level.

5→4, and 3→2 having time constants of 525, 740, 350, and 510 fs, respectively. The bottleneck state has a decay time of 12 ps.

Notice that the *a*602−*a*603 and *a*613−*a*614 dimers in our model are asymmetric, so the delocalization within the dimer is not uniform. Thus, the relative participations of the pigments in the exciton states are about 3:1. In the *a*610−*a*611−*a*612 trimer there is uniform delocalization over the *a*611−*a*612 pair with a coherent contribution from *a*610 which is bigger for the lower states, $k = 1$ and 5. A higher degree of delocalization leads to higher relaxation rates for the trimer.

For other realizations the rates may be different (by a factor of 1.5−2 or even more for some realizations); moreover, the ordering of states may be different. Thus, the kinetics averaged

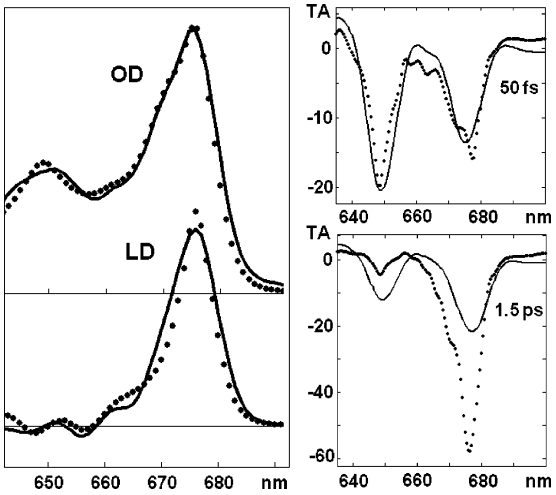

Figure 9. Experimental (points) and calculated (solid lines) OD, LD spectra, and TA profiles for a model with alternative exciton structure in the intermediate 660−670 nm region (see the text). TA spectra correspond to 50 fs and 1.5 ps delays after 650 nm excitation

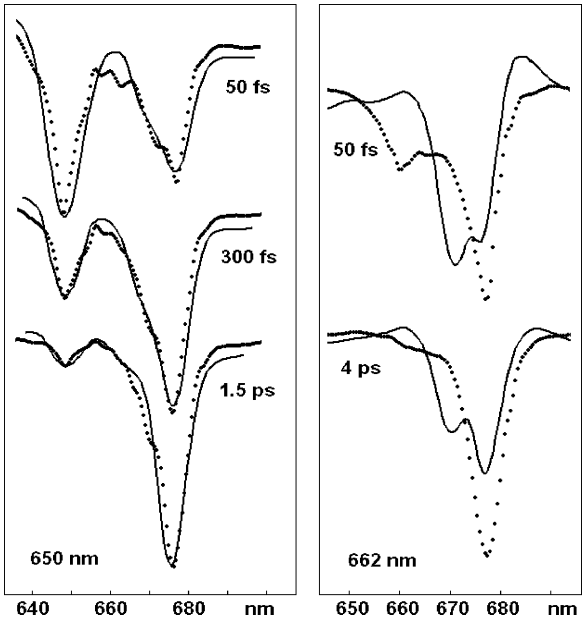

Figure 10. Experimental (points) and calculated (solid lines) TA profiles for a model with bottleneck *a*604 state shifted to the red (see the text). TA spectra correspond to 50 fs, 300 fs, and 1.5 ps upon 650 nm excitation (left frame) and 50 fs and 4 ps delays upon 662 nm excitation (right frame).

over disorder will reflect a noncoherent superposition of the states (for example the superposition of short- and long-lived states in the $k = 5-8$ region, etc.) and a mixed contribution from different relaxation pathways. Disorder will also reduce the degree of delocalization. Thus, the exciton structure (Figure 3) does not show the existence of highly supperradiant states. The superradiance of individual states does not exceed 1.5. The thermally averaged superradiance is 1.15 at 77 K (experiments[30] showed a value of 1.16).

In the *b* region fast relaxation within the *b* clusters (up to 100 fs) and sub-picosecond rates of the *b*→*a* transfer are obtained. These rates are also strongly dependent on the realizations of the disorder (and on the exciton structure of the *b* clusters).

Configurations with Other Site Energies. In preceding sections we have described the antenna model with specific site energies that allows a simultaneous fit of the experimental data. We have seen how this model works, i.e., which spectral forms (pigments or collective exciton states with a specific spectral positions) are responsible for any particular features of the steady-state spectra as well as for any particular time constants of the kinetics. Now we wish to illustrate what will happen if we use models with other site energies. As we point out above these models have been ruled out because they allow only a partial fit of the data. After detailed studies of the dynamics for our working model we can also understand why other configurations (with other site energies) fail to explain all the data.

We have seen that the Chl *b*→Chl *a* energy transfer in LHCII occurs via intermediate spectral forms including higher exciton states of the Chl *a* clusters and long-lived monomeric states. The exciton states are responsible for a fast conversion of energy from the 660−670 nm region to the lowest states of the *a* band. The monomeric states near 660−665 nm play the role of a bottleneck, giving rise to slow picosecond components. In the modeling the 660−670 nm region plays a decisive role. On the other hand it is very difficult to reproduce the OD and LD features near 660−670 nm. But the real problem is to find configurations consistent with the combined action of fast and slow transfers in this region.

As an example Figure 9 shows the model where the asymmetric *a*602−*a*603 dimer (as in our working model—see above) is replaced by a more symmetric one and shifted to the red. Thus, we remove one channel of fast energy conversion from 660 to 670 nm to the red-most states. Also we destroy delocalization within the *a*610−*a*611−*a*612 trimer by shifting the energy of *a*611 to the blue, which is expected to slow the intracluster relaxation. The position of the bottleneck *a*604 state is not changed. This configuration allows a good fit of the linear spectra (see OD and LD fits in Figure 9), but the TA kinetics upon 650 nm excitation becomes significantly slower (see the calculated 50 fs and 1.5 ps spectra in Figure 9 in comparison with the same spectra in Figure 4). This illustrates the importance of the channels of *b*→*a* transfer through the upper exciton levels of the *a* clusters in the intermediate region.

Figure 10 demonstrates what will happen if we shift the bottleneck *a*604 site from the intermediate region by 8 nm to the red. Normally this site contributes to the states with average position of the zero-phonon transitions at 665−670 nm (the corresponding low-frequency absorption maximum is about 2 nm red-shifted). The shifting of the *a*604 site to the red results in a decrease of absorption in the 662−668 nm region that can be compensated for by some blue shift of the upper levels of the *a* clusters. As a result we are still able to reproduce quantitatively the linear spectra (data not shown); moreover the TA kinetics upon 650 nm excitation correctly reproduce the main time constants of the *b*→*a* transfer (see left frame in Figure 10). But, the TA spectra upon 662 nm excitation are completely wrong in this case. The long-lived bleaching is now shifted to the region around 670 nm. This demonstrates that the position of the long-lived states is very important in the case of excitation in the intermediate region, as can be monitored in transient-absorption experiments.

We conclude that modeling of the excitation dynamics in LHCII is very critical with respect to variation of the site energies. This must also be the case for other similar complexes, which have (like LHCII) excited states with a different degree of delocalization, multiple pathways of energy transfer, and a variety of time scales of equilibration dynamics. The examples given in this section also show the importance of the simultaneous fit of steady-state spectra and kinetics upon different excitation conditions. Thus, any modeling based on a fragmen-

TABLE 4: Comparison of Chl Identities Used in Previous Studies Based on the Structure of Kühlbrandt et al. (1994)[2] and Identities Obtained by Liu et al.[26] [a]

1	2	3	4	5	6	7	8	9	10	11	12	13	14
b	a	a	a	b	b	b	b	b	a	a	a	a	a
	A4	A5	A6		B6	A7	B1	B5	A1	B2	A2	A3	B3
	a	a	*a*/*b*		b	*a*/*b*	a	b	a	b	a	*a*/*b*	*a*/*b*

[a] The first two lines show the numbers of the 14 pigments from 601 to 614 and their identities according to Liu et al.[26] The next two lines show notations of the 12 pigments of Kühlbrandt et al.,[2] and their identities according to Remelli et al.[3] Mixed sites are labeled as *a*/*b*. Notice that the new structure contains two Chls *b* (pigments 1 and 5) which were not present in the old structure.

tary part of the data (like a fit of only the linear spectra, or a fit of the kinetics at one wavelength, etc.) is not unique and therefore cannot give relevant information.

Discussion

In Table 4 a comparison is made between the Chl identities used in previous studies[10−12] and in the present model. In the old structure 12 Chls per monomeric subunit were found.[2] According to the original assignment[2] the sites A_{1-7} are occupied by Chls *a* and the sites $B_{1-3,5,6}$ by Chls *b*. Further site-directed mutagenesis studies[3−8] led to a different assignment. Thus, Remelli et al.[3] concluded that the sites A_1, A_2, A_4, A_5, and B_1 are occupied by Chls *a* and the sites B_2, B_5, and B_6 by Chls *b*, whereas A_3, A_6, A_7, and B_3 are mixed sites which can bind both Chls *a* and Chls *b*. This result was contested by Rogl and co-workers[4,6] who assumed that mixed binding sites cannot occur in native complexes and concluded that the A_3 and B_3 sites both bind Chl *a*. In a more recent assignment of Bassi [private communication] a Chl *b* is proposed to bind at site A_7, whereas the other three sites remain mixed. During 2001−2004 several theoretical studies have been performed,[10−12] using the identities proposed by Remelli et al. Thus, Iseri and Gülen[10] attempted to assign the orientations of the Chls by modeling the OD and LD spectra, supposing that all mixed sites have equal probability to bind Chl *a* or *b*, thus considering all 16 possible configurations of $A_3A_6A_7B_3$ from *aaaa* to *bbbb*. A simultaneous fit of OD, LD spectra, TA, TG, and 3PEPS kinetics with the Redfield theory was obtained with the $A_3A_6A_7B_3$ = *bbaa* and *baba* configurations.[11] Later a similar fit with the modified Redfield suggested $A_3A_6A_7B_3$ = *bbaa*, *baba*, *aabb*, and *abba* as possible configurations.[12] We supposed that these four configurations occur in the native antenna with equal probability, so that the sites A_3 and A_6 each bind on average 0.5 Chl *a* and 0.5 Chl *b*, and A_7 binds Chl *a* and Chl *b* in a ratio of 1:3, and B_3 in a ratio of 3:1. This is identical to the assignment $A_3A_6A_7B_3$ = *a*613*a*604*b*607*a*614 = *aaba* obtained in the new structure.

Another important point concerns the assignment of intermediate states. In our previous modeling we found that these bottleneck states are determined by two or three monomeric Chls *a* or *b* shifted to the spectral region between the main absorption peaks of Chl *b* and Chl *a*. An interesting conclusion was that these energy-shifted Chls are always (for all configurations) bound at mixed sites (i.e. A_3, A_6, A_7, or B_3). In the new structure this would correspond to a shift to an intermediate position of two to three pigments from the $A_3A_6A_7B_3$ = *a*613*a*604*b*607*a*614 group, i.e., a blue shift of one to two *a* sites *a*613, *a*604, or *a*614 and a red shift of *b* site *b*607. In fact, in our model based on the new structure the *a*604 and *a*614 are blue-shifted, whereas *b*605 and *b*607 are red-shifted (remember that *b*605 is an additional Chl *b*, found in the new structure). This is in remarkable agreement with the earlier mutagenesis studies, suggesting a blue shift of the B_3 (*a*614) site.[4,6] The most long-lived of these states are located on monomeric *a*604 and *b*605, both well-separated from other pigments of the trimeric complex.

Fast interband transfer determined in previous models by *b*−*a* heterodimers B_2-A_2, B_3-A_3, and B_5-A_5 (see ref 11) is now determined by other pigments. In the new structure both B_2-A_2 and B_3-A_3 are Chl *a* dimers. Only the heterodimer B_5-A_5 = *b*609−*a*603, having very strong coupling (see Figure 2), still contributes to the fast interband transfer. On the other hand B_1 (now *b* site *b*608) is strongly coupled to *a*610. There is also an additional Chl *b* (*b*601), which is strongly coupled to *a*611 and *a*602. These new *b* sites are now responsible for effective *b*−*a* connection.

Fast equilibration within the *a* band is determined by the same clusters as in the previous models; i.e., A_4-A_5 = *a*602−*a*603, $A_3(a)-B_3(a)$ = *a*613−*a*614, and $A_1-A_2-B_2$ = *a*610−*a*611−*a*612 (in the old structure it was $A_1-A_2-B_1$, but in the new structure the B_2 and B_1 pigments closely connected to the A_1-A_2 group change their identities). The lowest state of the *a* band is a coherent exciton state of the *a*610−*a*611−*a*612 trimer. Notice that the mutagenesis studies with removed A_2 (*a*612) showed a pronounced contribution of this pigment to the red-most state.[4,6] This is also the case in our model, but the contribution to the lowest state of *a*610 is still bigger than that of *a*612.

Fast dynamics within the *b* region is determined by fast relaxation within the strongly coupled dimers *b*606−*b*607 (also present in previous models) and *b*608−*b*609, which now appeared due to the change of the B_1 identity in the new crystal structure.

We conclude that the origin of fast intra- and interband dynamics and the nature of the long-lived intermediate states are basically the same as in previous models based on the previous structure.[11,12] Moreover, the assignment of the fast relaxation channels and bottleneck states are also not much different from those proposed by earlier modeling.[11,12] On the other hand there are several new pathways due to changing of identities of the B_2 and B_1 pigments and due to the existence of two additional *b* sites.

A great advantage of the new structure is the assignment of the Chl orientations and identities. In previous models many possible configurations with different site energies, identities, and orientations have been proposed, whereas now only the site energies remain as free parameters. Moreover there is only one monomeric Chl *a* in the new structure, i.e., only one good candidate for a really long-lived bottleneck state. Due to this fortunate circumstance the whole set of the site energies can be better defined from a simultaneous fit of the linear and nonlinear spectral responses.

Conclusions

We have modeled steady-state spectra and energy-transfer dynamics of the peripheral plant light-harvesting complex LHCII

using new structural data, which allowed an assignment of the identities and orientations of the Chls. The dynamics of the chlorophyll (Chl) *b*→Chl *a* transfer and the decay of selectively excited bottleneck Chl *a* states have been studied by femtosecond pump−probe spectroscopy. A quantitative simultaneous fit of the absorption (OD), linear dichroism (LD), steady-state fluorescence (FL) spectra, and transient absorption (TA) kinetics upon excitation at different wavelengths allowed us to determine the site energies of the 14 Chls within a monomeric subunit. Knowledge of the site energies and the experimental exciton−phonon spectral density makes it possible to determine pathways and time scales of energy transfer in the system. We have found that fast *b*→*a* transfer is determined by a good connection of the Chls *b* to strongly coupled Chl *a* clusters, i.e., *a*610−*a*611−*a*612 trimer and *a*602−*a*603 and *a*613−*a*614 dimers. Slow components of the energy-transfer kinetics are determined by a quick population of blue-shifted monomeric Chl *a*604 followed by a very slow (12 ps) flow of energy from this bottleneck site to the remaining *a* sites. Dynamics within the Chl *a* region is determined by fast (with time constants up to sub-100 fs) exciton relaxation within the *a*610−*a*611−*a*612 trimer, slower 200−300 fs relaxation within *a*602−*a*603 and *a*613−*a*614 dimers, even slower 300−800 fs migration between these clusters, and very slow transfer from *a*604 to the quasi-equilibrated *a* sites. The excited-state equilibrium is characterized by predominant population of the *a*610−*a*611−*a*612 cluster (mostly the *a*610 site). The location of this cluster at the outer side of the LHCII trimer provides a better connection with other subunits of PSII. The current modeling with state-of-the-art physical theory provides a good description of the steady-state and time-resolved spectroscopy of LHCII in terms of the new crystal structure.

Acknowledgment. V.I.N. was supported by The Netherlands Organization for Scientific Research (NWO; Dutch−Russian scientific cooperation program, Grant 047.016.006), a visitor's grant from NWO (2004), and by the Russian Foundation for Basic Research, Grant No. 02-04-48779.

References and Notes

(1) van Amerongen, H.; van Grondelle, R. *J. Phys. Chem. B* **2001**, *105*, 604.
(2) Kühlbrandt, W.; Wang, D. N.; Fujiyoshi, Y. *Nature* **1994**, *367*, 614.
(3) Remelli, R.; Varotto, C.; Sandona, D.; Croce, R.; Bassi, R. *J. Biol. Chem.* **1999**, *274*, 33510.
(4) Rogl, H.; Kühlbrandt, W. *Biochemistry* **1999**, *38*, 16214.
(5) Yang, C.; Kosemund, K.; Cornet, C.; Paulsen, H. *Biochemistry* **1999**, *38*, 16205.
(6) Rogl, H.; Schödel, R.; Lokstein, H.; Kühlbrandt, W.; Schubert, A. *Biochemistry* **2002**, *41*, 2281.
(7) Bassi, R.; Croce, R.; Cugini, D.; Sandonà, D. *Procl. Natl. Acad. Sci. U.S.A.* **1999**, *96*, 10056.
(8) Simonetto, R.; Crimi, M.; Sandonà, D.; Croce, R.; Cinque, G.; Breton, J.; Bassi, R. *Biochemistry* **1999**, *38*, 12974.
(9) Renger, Th.; May, V. *Phys. Rev. Lett.* **2000**, *84*, 5228.
(10) Iseri, E. I.; Gülen, D. *Eur. Biophys. J.* **2001**, *30*, 344.
(11) Novoderezhkin, V.; Salverda, J. M.; van Amerongen, H.; van Grondelle, R. *J. Phys. Chem. B* **2003**, *107*, 1893.
(12) Novoderezhkin, V.; Palacios, M.; van Amerongen, H.; van Grondelle, R. *J. Phys. Chem. B* **2004**, *108*, 10363.
(13) Bittner, T.; Wiederrecht, G. P.; Irrgang, K.-D.; Renger, G.; Wasielewski, M. R. *Chem. Phys.* **1995**, *194*, 311.
(14) Visser, H. M.; Kleima, F. J.; van Stokkum, I. H. M.; van Grondelle, R.; van Amerongen, H. *J. Chem. Phys.* **1996**, *210*, 297.
(15) Kleima, F. J.; Gradinaru, C. C.; Calkoen, F.; van Stokkum, I. H. M.; van Grondelle, R.; van Amerongen, H. *Biochemistry* **1997**, *36*, 15262.
(16) Gradinaru, C. C.; Özdemir, S.; Gülen, D.; van Stokkum, I. H. M.; van Grondelle, R.; van Amerongen, H. *Biophys. J.* **1998**, *75*, 3064.
(17) Gradinaru, C. C.; van Stokkum, I. H. M.; Pascal, A. A.; van Grondelle, R.; van Amerongen, H. *J. Phys. Chem. B* **2000**, *104*, 9330.
(18) Du, M.; Xie, X.; Mets, L.; Fleming, G. R. *J. Phys. Chem.* **1994**, *98*, 4736.
(19) Bittner, T.; Irrgang, K.-D.; Renger, G.; Wasielewski, M. R. *J. Phys. Chem.* **1994**, *98*, 11821.
(20) Connelly, J. P.; Müller, M. G.; Hucke, M.; Gatzen, G.; Mullineaux, C. W.; Ruban, A. V.; Horton, P.; Holzwarth, A. R. *J. Phys. Chem. B* **1997**, *101*, 1902.
(21) Agarwal, R.; Krueger, B. P.; Scholes, G. D.; Yang, M.; Yom, J.; Mets, L.; Fleming, G. R. *J. Phys. Chem. B* **2000**, *104*, 2908.
(22) Salverda, J. M.; Vengris, M.; Krueger, B. P.; Scholes, G. D.; Czarnoleski, A. R.; Novoderezhkin, V.; van Amerongen, H.; van Grondelle, R. *Biophys. J.* **2003**, *84*, 450.
(23) Redfield, A. G. *Adv. Magn. Reson.* **1965**, *1*, 1.
(24) Pollard, W. T.; Felts, A. K.; Friesner, R. A. *Adv. Chem. Phys.* **1996**, *93*, 77.
(25) Zhang, W. M.; Meier, T.; Chernyak, V.; Mukamel, S. *J. Chem. Phys.* **1998**, *108*, 7763.
(26) Liu, Z.; Yan, H.; Wang, K.; Kuang, T.; Zhang, J.; Gui, L.; An, X.; Chang, W. *Nature* **2004**, *428*, 287.
(27) Knox, R. S.; Spring, B. Q. *Photochem. Photobiol.* **2003**, *77* (5), 497.
(28) Peterman, E. J. G.; Pullerits, T.; van Grondelle, R.; van Amerongen, H. *J. Phys. Chem. B* **1997**, *101*, 4448.
(29) van Amerongen, H.; Kwa, S. L. S.; van Bolhuis, B. M.; van Grondelle, R. *Biophys. J.* **1994**, *67*, 837.
(30) Palacios, M. A.; de Weerd, F. L.; Ihalainen, J. A.; van Grondelle, R.; van Amerongen, H. *J. Phys. Chem. B* **2002**, *106*, 5782.
(31) Nussberger, S.; Dekker, J. P.; Kühlbrandt, W.; van Bolhuis, B. W.; van Grondelle, R.; van Amerongen, H. *Biochemistry* **1994**, *33*, 14775.
(32) Peterman, E. J. G.; Hobe, S.; Calkoen, F.; van Grondelle, R.; Paulsen, H.; van Amerongen, H. *Biochim. Biophys. Acta* **1996**, *1273*, 171.